

How large are temporal representativeness errors in paleoclimatology?

Dan Amrhein

November 19, 2018

Abstract

Ongoing work in paleoclimate reconstruction and model-data comparison prioritizes understanding the origins and magnitudes of paleoclimate data errors. One class of such errors arises from assumptions of proxy temporal representativeness – i.e., the time scales over which climate variables are equated with paleoclimate proxy measurements. This paper addresses errors that arise when a proxy estimate of a mean value over a “measurement duration” τ_y is used to represent time-mean climate conditions over a different “target duration” τ_x . Because it is challenging to tailor proxy measurements to precise time intervals, such errors are ubiquitous in model-data and data-data comparisons, but it is not always clear how important these errors are. Moreover, because values of τ_y are often not published alongside paleo data, amplitudes of these errors may be poorly constrained.

Here we show how time-mean representativeness errors depend on τ_x , τ_y , and the spectrum of the climate signal being sampled. Additional effects from record smoothing (due e.g. to bioturbation in sediment cores) and chronological offsets and uncertainties (e.g. arising from radiocarbon dating) are also considered. In some cases, particularly for small values of τ_x relative to τ_y , errors can be large relative to paleoclimatological signals of interest. As climate signal spectra become more dominated by low frequencies, the fraction of error variance decreases in observations. Comparisons reveal that errors have magnitudes that are comparable to those expected from chronological uncertainty. Smoothing in paleoclimate archives can reduce the effects of aliasing but also destroys high-frequency information. For paleoclimate time series, which are sequences of time-average values, measurement intervals shorter than the spacing between samples lead to errors, absent compensating effects from archive smoothing. Including these sources of uncertainty will improve accuracy in model-data comparisons and data comparisions and syntheses. Reporting sampling procedures, smoothing time scales, and chronological uncertainties alongside published data will facilitate quantifying uncertainty.

1 Introduction

³² Paleoclimate records provide important information about the variability, extremes, and sensitivity
³³ of Earth's climate to greenhouse gases on time scales longer than the instrumental period. As the

34 number of published paleoclimate records has grown and the sophistication of numerical model
35 representations of past climates has improved, it has become increasingly important to understand
36 the uncertainty with which paleoclimate observations represent climate variables, so that they can
37 be compared to one another and to model output. Additionally, quantifying uncertainty is important
38 for ongoing efforts to assimilate paleoclimate data with numerical climate models (e.g., ??).

39 Paleoclimate records can have errors arising from many different sources: biological effects
40 (e.g., ??), aliasing onto seasonal cycles (???), spatial representativeness (?), proxy-climate cali-
41 brations (e.g., ?), and instrument errors, to name a few. This paper focuses on errors from tem-
42 poral representativeness (TR), which we define as the degree to which a measurement averaging
43 over one time interval can be used to represent a second, target time interval – for instance, when
44 a decadal-average proxy is compared to a one-year average of model output. Errors in tempo-
45 ral representativeness can result both from systematic errors (e.g., knowingly using data from a
46 short period to represent a longer one) and from stochastic uncertainties in the duration and age of
47 paleoclimate observations that can originate, e.g., from uncertain radiocarbon age measurements.

48 Much of the previous study of errors arising from sampling in time has focused on aliasing,
49 whereby variability at one frequency in a climate process appears at a different frequency in dis-
50 crete samples of that process. ? described consequences of aliasing in the study of deterministic
51 peaks in climate spectra due to Milankovich forcing. ? described criteria for choosing sample
52 spacing so as not to alias low-frequency variability in sediment cores, and ? demonstrated how
53 aliasing can lead to spurious spectral peaks in ice core records. ? and ? describe how running
54 means can reduce aliasing of solar cycle variability in ice core records. In paleoclimate, measure-
55 ments are often unevenly spaced in time due to changes in archive deposition rates; ? showed that
56 aliasing is present and even exacerbated in unevenly-sampled records relative to regularly sampled
57 ones. Bioturbation and other diagenetic processes smooth records in time (??) and may act as
58 anti-aliasing filters.

59 A second area of previous focus stems from chronological uncertainties, whereby times as-
60 signed to measurements may be biased or uncertain. In some cases, such as for radiocarbon dat-

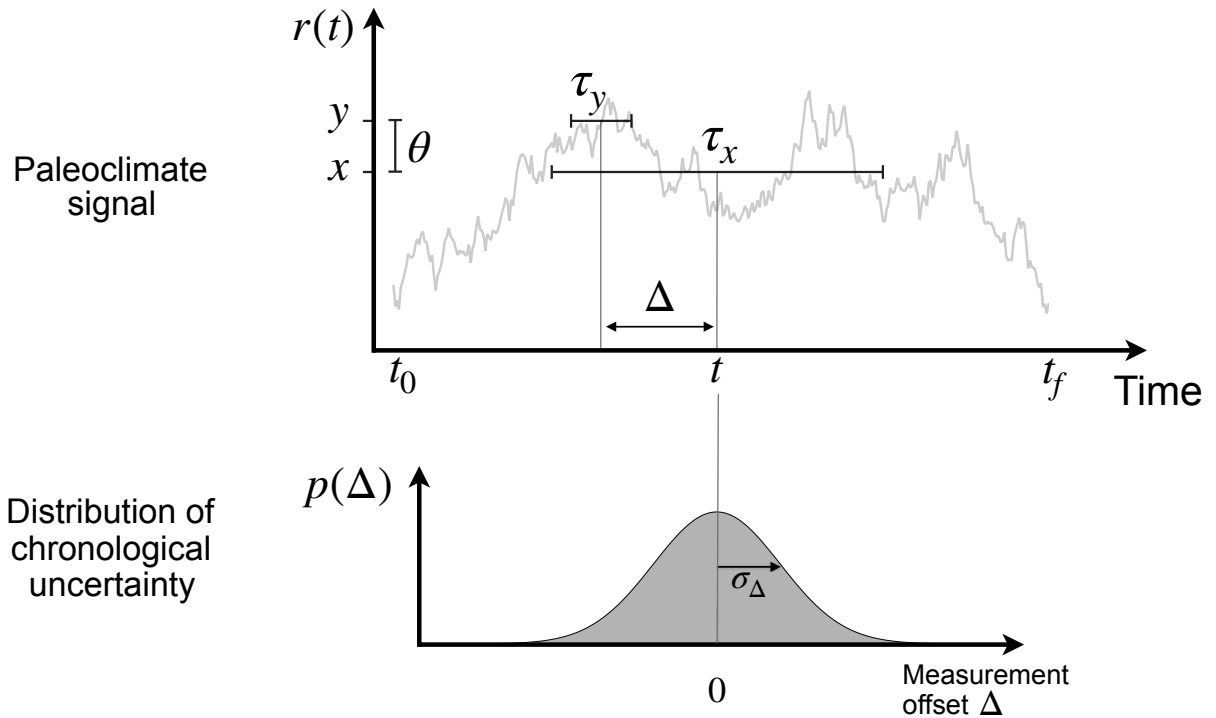


Figure 1: Schematic of temporal representativeness errors. When a target time-average quantity (x) of a paleoclimate signal ($r(t)$) is estimated using an observation (y), an error (θ) results if the averaging interval of the observation (τ_y) is different from that of the target period (τ_x), including a nonzero offset (Δ) between the centers of the two time averages. When a measurement is affected by chronological uncertainty, Δ is characterized by a probability distribution ($p(\Delta)$) of possible offsets, parameterized in this paper as a Gaussian with standard deviation σ_Δ . This paper characterizes the amplitude of θ as a function of time scales arising from 1) sampling procedures, 2) variability in $r(t)$, 3) archive smoothing, and 4) chronological uncertainty.

ing, estimates of these uncertainties are available from sophisticated Bayesian approaches (??);
 practices for incorporating this information into model-data or data-data comparisons vary, and
 developing tools for analyzing chronological uncertainty is an active area of research. ? include
 the effect of uncertainties in tie points in order to align multiple records of Pleistocene oxygen
 isotopes, and ? developed tools for estimating the statistics of time-uncertain series. The effect
 of time uncertainty on estimates of signal spectra is modest in some cases (?), in part because
 time uncertainty acts to smooth high-frequency variability when computed as an expectation over
 a record (?).

69 This paper uses an analytical model to quantify TR errors, including some effects from chrono-
70 logical uncertainty, and illustrate their dependence on signal spectra and sampling time scales. We
71 define TR errors generally as those arising when a time average over one interval is represented
72 as another interval (Figure ??). Such errors can arise when averages are computed over different
73 lengths of time, when intervals are offset to be centered on different times, and when those off-
74 sets are stochastic (chronological uncertainty). The work can be thought of as a quantification of
75 aliasing, specifically onto the zero frequency (the time mean). Extending results from time-mean
76 measurements to time series demonstrates how sampling practices can lead to aliasing errors when
77 records are not sampled densely, i.e. when an ocean sediment core is not sampled continuously or
78 densely along its accumulation axis. While we do not claim that TR error is the most important
79 source of uncertainty in paleoclimate records, it does appear to be large enough to affect results in
80 some cases. Moreover, this work is a step towards reducing the number of “unknown unknowns”
81 in paleoclimate reconstruction.

82 The rest of the paper is as follows. Section 2 describes a statistical model for time representa-
83 tiveness errors in time mean values. Section 3 illustrates the model by applying it to the analysis
84 of Last Glacial Maximum climate properties. Section 4 extends the model to the analysis of time
85 series. Implications, caveats, and future research questions appear in the Discussion. Table (??)
86 provides a glossary of functions and variables used.

87 **2 A statistical model for temporal representativeness errors**

88 In paleoclimatology, a common focus is computing the mean of a climate variable (sea surface
89 temperature, for instance, or isotope ratios, or global ice volume) over a particular time period
90 (for example, a marine isotope stage). Often computing a mean is the implicit goal of binning
91 procedures that combine observations from within a time period. This section defines an analytical
92 approach for estimating magnitudes of errors that arise in representing a time mean by a paleo-
93 climate measurement that represent a different time period than the target. These errors have a
94 compact representation in the frequency domain that allows us to understand the relative impor-

Variable	Meaning
t	Time
t_0	Initial time in a time series
t_f	Final time in a time series
v	Frequency
v_{Nyq}	Nyquist frequency
\hat{v}_{low}^{\dagger}	Lower cutoff frequency
\hat{v}_{high}^{\dagger}	Upper cutoff frequency
$r(t)$	Time-varying climate process
$m(t, \tau)$	Time mean of $r(t)$ over period τ centered on t
x	Target paleoclimate quantity
y	Measured paleoclimate quantity
θ	Error in representing x by y
τ_x	Averaging timescale of target quantity
τ_y	Averaging timescale of observation
τ_a	Timescale of archive smoothing
τ_s	Time interval between samples in a series
τ_0	Time series length (equal to $t_f - t_0$)
τ_c	Time between two time means being compared
Δ	Measurement time offset
σ_{Δ}	Standard deviation of chronological error
σ_{τ_c}	Expected difference between two time means separated by τ_c
$\Pi(t, \tau)$	Boxcar function in time
$G(v, \tau)$	Heaviside function in frequency
$H(v)$	Power transfer function
f	Error variance fraction
β	Spectral slope (times -1)

Table 1: Glossary of functions and variables. Variables denoted by a superscript i in the text denote the i^{th} value of that quantity in a time series. Fourier transformed variables are denoted by a hat (e.g., $\hat{r}(v)$).

95 tance and interaction of sampling procedures, time uncertainty, and signal spectra in contributing
96 to errors.

97 This approach is intended to be complementary to the output from proxy system models (PSMs;
98 e.g., ?) that relate proxy quantities to climate variables. These methods may be used to provide
99 an estimate of TR uncertainty when PSMs do not; when they do, the model, which is relatively
100 simple, may provide a framework for understanding the results. The starting point for the model
101 is a hypothetical climate process, $r(t)$, which we assume to be able to sample directly. We ignore
102 additional errors that are inherited from the construction of $r(t)$ from proxy observations. Vari-
103 ances from multiple error sources can be added together under the approximations that they are
104 independent and Gaussian. When thses assumptions fail, more holistic forward modeling of errors
105 may be necessary.

106 2.1 Errors in time-mean values

107 Define a mean value $m(t, \tau)$ of a climate variable $r(t)$ as a function of the duration τ and the time
108 t on which that duration is centered,

$$m(t, \tau) = \int_{-\infty}^{\infty} \Pi(t', \tau) r(t + t') dt', \quad (1)$$

109 where $\Pi(t, \tau)$ is a normalized “boxcar” function centered on $t = 0$ with width τ ,

$$\Pi(t, \tau) = \begin{cases} 1/\tau & |t| \leq \tau/2 \\ 0 & |t| > \tau/2. \end{cases} \quad (2)$$

110 The operation in (??) defines a moving average $m(t, \tau)$ and is known as a convolution, hereafter
111 denoted as a star,

$$m(t, \tau) = \Pi(t, \tau) \star r(t). \quad (3)$$

Our focus is on errors that arise when a mean value computed over one time period is used to

represent another time period – for instance, when a time average over over 20-19 kya (thousand years ago) is used to represent an average over 23-19 kya, the nominal timing of the Last Glacial Maximum (?). To write this representation generally, define a target quantity to be a mean x of $r(t)$ over an interval of length τ_x centered on t , and an observation y to be an average over a different duration τ_y centered on a different time $t + \Delta$,

$$x = m(t, \tau_x) \quad (4)$$

$$y = m(t + \Delta, \tau_y). \quad (5)$$

112 (While these quantities are functions of several variables, we write them simply as x and y for
113 brevity.) In many cases, paleoclimate archive are smoothed prior to processing by bioturbation,
114 diagenesis, residence times in karst systems upstream of speleothems, or other effects. These
115 processes can be complex and non-constant in time; here, to gain a basic understanding of their
116 effects, we assume an archive smoothing process that is a moving average over a time scale τ_a .
117 Under such smoothing, we can then write y as a twice-smoothed function of $r(t)$,

$$y = \Pi(t, \tau_y) * \Pi(t, \tau_a) * r(t)$$

TR error is defined as the error in representing x by y ,

$$\theta = x - y \quad (6)$$

118 We will characterize θ by estimating its variance, $\langle (\theta - \langle \theta \rangle)^2 \rangle$, where angle brackets denote
119 statistical expectation. This approach assumes that $r(t)$ is weakly statistically stationary, meaning
120 that its mean and variance do not change in time; caveats surrounding this assumption are addressed
121 later in the paper. Under the weak stationarity assumption, the mean error $\langle \theta \rangle$ is zero, and we take

122 the expectation by evaluating θ^2 at all the times in $r(t)$ to compute the variance,

$$\langle \theta^2 \rangle = \frac{1}{\tau_0} \int_{t_0}^{t_f} (x - y)^2 dt, \quad (7)$$

123 where t_0 and t_f are the intial and final times in $r(t)$, and $\tau_0 = t_f - t_0$.

Intuitively, we are estimating the error in representing x by y (*at a single time*) as the time-mean squared difference of running means of $r(t)$. In practice, though we do not know $r(t)$, knowledge of its statistics is adequate to estimate $\langle \theta^2 \rangle$. To show this, define $x' = x - \langle x \rangle$ and $y' = y - \langle y \rangle$, where $\langle x \rangle = \langle y \rangle$ for stationary $r(t)$. Then expanding (??) gives an expression in terms of estimated variances $\tilde{\sigma}_x^2$ and $\tilde{\sigma}_y^2$ and the cross-covariance a function of lag Δ , $\tilde{C}_{xy}(\Delta)$:

$$\langle \theta^2 \rangle = \frac{1}{\tau_0} \int_{t_0}^{t_f} (x' - y')^2 dt \quad (8)$$

$$= \frac{1}{\tau_0} \left(\int_{t_0}^{t_f} x'^2 dt + \int_{t_0}^{t_f} y'^2 dt - 2 \int_{t_0}^{t_f} x' y' dt \right) \quad (9)$$

$$= \tilde{\sigma}_x^2 + \tilde{\sigma}_y^2 - 2\tilde{C}_{xy}(\Delta). \quad (10)$$

124 In the limit where $\tau_x = \tau_y$ and $\Delta = 0$, $\tilde{\sigma}_x^2 = \tilde{\sigma}_y^2 = \tilde{C}_{xy}(\Delta)$, and $\langle \theta^2 \rangle = 0$, as we would expect for
125 the case where the measurement exactly targets the quantity of interest. If $\tilde{C}_{xy}(\Delta) = 0$ – i.e., the
126 measurement and target quantity are uncorrelated – then y has no skill in representing x , and the
127 error variance is the sum of $\tilde{\sigma}_x^2$ and $\tilde{\sigma}_y^2$. If there is a choice of Δ such that x and y are anticorrelated,
128 then $\tilde{C}_{xy}(\Delta)$ will be negative, leading to still larger errors. Between these extremes of zero and
129 maximum error, intermediate values of $\langle \theta^2 \rangle$ are set by timescales of sampling (τ_x , τ_y , and Δ) and
130 variability in $r(t)$. We can understand these relationships by representing TR error in the frequency
131 domain.

₁₃₂ **2.2 Analyzing sources of error in the frequency domain**

₁₃₃ Using Parseval's theorem, the Fourier shift theorem, and the convolution theorem (Appendix A),
₁₃₄ denoting frequency by v , and denoting the Fourier transform by a hat, we can transform (??) into
₁₃₅ the frequency domain as

$$\langle \theta^2 \rangle = \frac{1}{\tau_0} \int_0^\infty \left| \hat{\Pi}(v, \tau_x) - e^{-2\pi i v \Delta} \cdot \hat{\Pi}(v, \tau_a) \cdot \hat{\Pi}(v, \tau_y) \right|^2 |\hat{r}(v)|^2 dv. \quad (11)$$

₁₃₆ The integrand of (??) is the product of two components. The second, $|\hat{r}(v)|^2$, is the power spectral
₁₃₇ density of $r(t)$, which describes the variance contained at frequencies in $r(t)$. The first component
₁₃₈ is a so-called power transfer function,

$$H_{\tau_s, \tau_d, \tau_y, \Delta}(v) = \left| \hat{\Pi}(v, \tau_s) - e^{-2\pi i v \Delta} \cdot \hat{\Pi}(v, \tau_a) \cdot \hat{\Pi}(v, \tau_y) \right|^2, \quad (12)$$

₁₃₉ which describes how power at different frequencies in $r(t)$ contributes to $\langle \theta^2 \rangle$. To understand
₁₄₀ which frequencies contribute most, first note that the Fourier transform of the boxcar function is a
₁₄₁ sinc function,

$$\hat{\Pi}(v, \tau) = \text{sinc}(\tau v) = \frac{\sin(\pi \tau v)}{\pi \tau v}, \quad (13)$$

₁₄₂ which converges to 1 at low frequencies and oscillates with decreasing amplitude about 0 at higher
₁₄₃ frequencies, with the first zero crossing at $1/\tau$ (Figure ??a). The largest values in H , which con-
₁₄₄ tains a squared difference of sinc functions, lie roughly within a frequency band (Figure ??b).

In some cases, the edges of this band can be estimated using simple functions of the sampling time scales. Define the low and high cutoff frequencies v_{low}^\dagger and v_{high}^\dagger as the lower and higher frequencies where the power transfer function is 0.5 flanking the band of nonzero values. When τ_x and τ_y are sufficiently separated (roughly $\tau_x \geq 4\tau_y$), and in the absence of time offsets ($\Delta = 0$), we

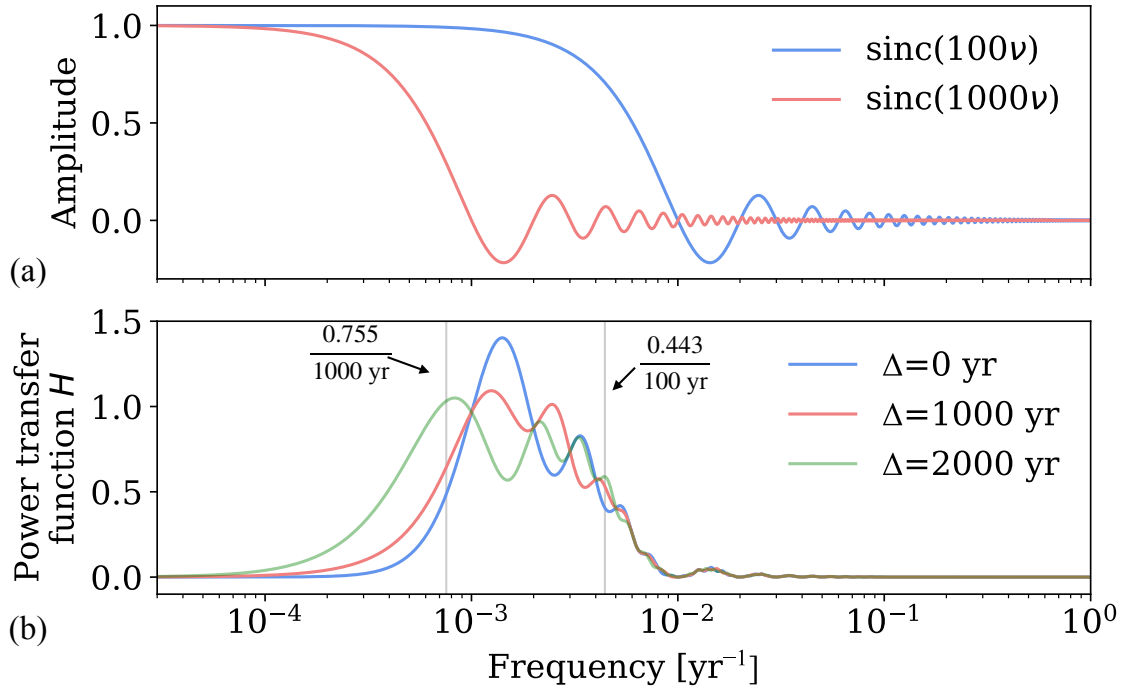


Figure 2: Contributions to the power transfer function H (Equation ??) illustrate the dependence of temporal representativeness errors on sampling time scales. (a) The Fourier transform of the boxcar function (Equation ??) is the sinc function (Equation ??), illustrated here for $\tau = 100$ and $\tau = 1000$. (b) Power transfer function computed with $\tau_x = 1000$, $\tau_y = 100$, and three different values of the time offset Δ . When $\Delta = 0$, Equations (??) and (??) approximate the edges of the frequency band in $r(t)$ that is aliased onto errors θ . For nonzero Δ , errors originate from frequencies as low as $1/(2\Delta)$.

can estimate the cutoff frequencies by solving

$$\left| 1 - \text{sinc}^2 \left(\tau v_{low}^\dagger \right) \right|^2 = \frac{1}{2} \quad (14)$$

$$\left| \text{sinc} \left(\tau v_{high}^\dagger \right) \right|^2 = \frac{1}{2} \quad (15)$$

¹⁴⁵ yielding $v_{low}^\dagger = 0.755\tau^{-1}$ and $v_{high}^\dagger = 0.443\tau^{-1}$. When τ_x is less than τ_y , then these time scales
¹⁴⁶ should be switched in (??) and (??). For values of τ_x and τ_y that are closer together, the complex
¹⁴⁷ shape of the sinc function necessitates plotting H to diagnose frequency limits.

¹⁴⁸ If the paleoclimate archive was smoothed prior to sampling, then v_{high}^\dagger can be estimated by

¹⁴⁹ solving

$$\left| \text{sinc} \left(\tau_a v_{high}^\dagger \right) \text{sinc} \left(\tau_y v_{high}^\dagger \right) \right|^2 = \frac{1}{2}; \quad (16)$$

¹⁵⁰ using a Taylor series representation gives the approximate formula

$$v_{high}^\dagger = \frac{0.443}{\sqrt{\tau_a^2 + \tau_y^2}}, \quad (17)$$

¹⁵¹ which combines effects from sampling and archive smoothing. One can estimate an ideal length
¹⁵² $\tilde{\tau}_y$ to minimize error for $\tau_x > \tau_a$ by setting $0.443 \tilde{\tau}_x^{-1} = 0.443 (\tau_y^2 + \tau_a^2)^{-\frac{1}{2}}$ and solving, yielding

$$\tilde{\tau}_y = \sqrt{\tau_x^2 - \tau_a^2} \text{ for } \tau_x > \tau_a. \quad (18)$$

¹⁵³ Whether this approach is useful given the complexity of archive smoothing processes will depend
¹⁵⁴ on the application.

¹⁵⁵ Finally, when there is a time offset, the band of nonzero values in H can extend to frequencies
¹⁵⁶ as low as $1/2\Delta$, with sinusoidal variations at time scales set by Δ (Figure ??d; Appendix A).
¹⁵⁷ Chronological uncertainty in paleoclimate measurements can be expressed by allowing Δ to be
¹⁵⁸ a random variable with probability distribution $p(\Delta)$. Given chronological uncertainty, we can
¹⁵⁹ compute a typical value for $\langle \theta^2 \rangle$ by computing the expectation over $p(\Delta)$, denoted with a second
¹⁶⁰ pair of angle brackets,

$$\langle\langle \theta^2 \rangle\rangle = \int_{-\infty}^{\infty} p(\Delta) \langle \theta^2 \rangle d\Delta. \quad (19)$$

¹⁶¹ 2.3 Implications for time-mean representational errors

¹⁶² Given estimates of the sampling interval, archive smoothing time scale, measurement offset, and
¹⁶³ an estimate of the signal spectrum, (??) is a closed-form expression for estimating TR errors in
¹⁶⁴ time-mean estimates. This equation provides a basis for some intuitive conclusions about errors
¹⁶⁵ and their implications for record sampling and uncertainty quantification:

- 166 1. TR errors can be traced to variability within a frequency band in $r(t)$ that is aliased onto
 167 time means. For instance, if a centennial mean is used to represent a millennial mean, in the
 168 absence of archive smoothing, the expected error variance is equal to the variance in $r(t)$ at
 169 periods between 226 and 1325 years (Figure ??). The error is the same if a centennial mean
 170 is used to represent a decadal mean.
- 171 2. The combined effects of archive smoothing and sampling can lead to over-smoothing. For
 172 instance, choosing a sampling interval τ_y equal to τ_x when $\tau_a > 0$ will over-smooth a record
 173 and lead to errors because the observed quantity averages over a longer interval than the
 174 target.
- 175 3. When there is a time offset in the measurement relative to the target, additional variability is
 176 aliased onto errors.

177 3 Application: Estimating errors at the Last Glacial Maximum

178 Next the error model is applied in the context of a particular mean estimation problem: the Last
 179 Glacial Maximum (LGM), the period roughly 20,000 years ago that is associated with the greatest
 180 land ice extent during the last glacial period. Following ? and others, LGM properties are defined
 181 to be estimates of time means over the 4000-year-long period from 23,000 to 19,000 years ago
 182 (23-19 kya). To estimate LGM errors, we will estimate the typical errors that would arise in the
 183 case of representing a 4000-year long interval centered on 21 kya.

184 Denote the time-mean value of a climate quantity $r(t)$ during the LGM as the target quantity

185 x_{LGM} ,

$$x_{LGM} = \frac{1}{4000} \int_{-23,000}^{-19,000} r(t) dt.$$

186 To illustrate TR errors, we will compare averages over different time periods to x_{LGM} . For instance,

¹⁸⁷ consider a 1000-year time-mean value of $r(t)$ centered on 19.5 kya,

$$y_{LGM} = \frac{1}{1000} \int_{-19,000}^{-20,000} r(t) dt. \quad (20)$$

¹⁸⁸ Such an estimate – dated to within the LGM, but averaging over only a subset – could reasonably
¹⁸⁹ be included in a binned-average compilation of LGM data. However, without accounting for errors
¹⁹⁰ resulting from the short averaging interval and time offset from the center of the LGM, we would
¹⁹¹ expect this observation to bias a binned average. Similarly, were we to compare y_{LGM} to an LGM-
¹⁹² mean estimate of $r(t)$ from a model without taking TR errors into account, we might erroneously
¹⁹³ conclude that the model did not fit the data.

¹⁹⁴ To compare the effects of various time scales and spectra it is helpful to analyze a normalized
¹⁹⁵ function of $\langle \theta^2 \rangle$: the noise-to-signal standard deviation ratio,

$$f = \frac{\sqrt{\langle \theta^2 \rangle}}{\sigma_{\tau_c}}. \quad (21)$$

¹⁹⁶ Because a common goal of LGM reconstructions is estimating glacial differences from modern
¹⁹⁷ climate, we adopt as our “signal” amplitude the expected anomaly σ_{τ_c} between two mean intervals
¹⁹⁸ of length τ_x separated by a time τ_c , where $\tau_c = 21,000$ years.

¹⁹⁹ 3.1 Analysis of errors by subsampling a high-resolution paleoclimate record

²⁰⁰ To study the sensitivities of TR errors to sampling time scales, we first compare different sub-
²⁰¹ samplings of a high-resolution climate record, the North Greenland Ice Core Project (NGRIP; ?)
²⁰² 50-year average time series of oxygen isotope ratios ($\delta^{18}\text{O}$) of ice. Smoothing this record with
²⁰³ running means of length $\tau_x = 4000$ and $\tau_y = 1000$ yields time series of target and observation val-
²⁰⁴ ues x and y (black and red lines, Figure 3a). Their difference is the error θ (thick black line, Fig.
²⁰⁵ 3a); the mean $\langle \theta^2 \rangle$ (red line, Figure 3b) of θ^2 (blue line, Fig. 3b) is $0.7 (\text{‰} \delta^{18}\text{O})^2$ and is our
²⁰⁶ estimate of the error variance (corresponding to a typical deviation of $\sqrt{\langle \theta^2 \rangle} = 0.8\text{‰}$). Errors in

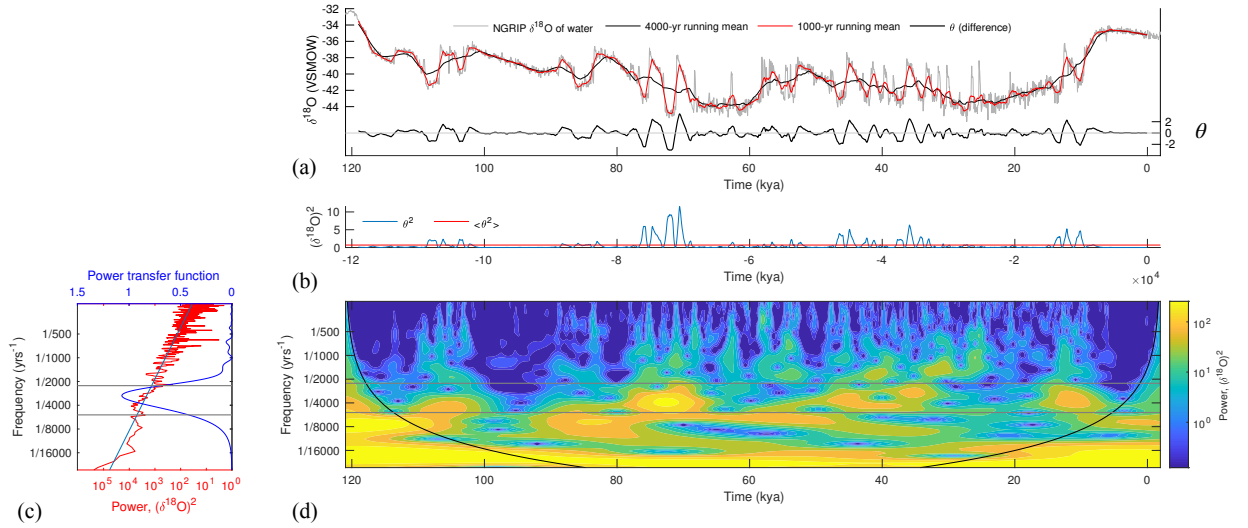


Figure 3: Temporal representativeness error in the time and frequency domains. Errors in representing a 4000-year mean by a 1000-year mean are estimated by computing the difference θ ((a), thick black line) between a 4000-year (red line) and 1000-year (thin black line) running mean of the NGRIP $\delta^{18}\text{O}_{\text{ice}}$ record (grey). The time average (red line, (b)) of θ^2 (blue line) is an estimate (0.7, units of $(\text{‰} \delta^{18}\text{O})^2$) of the temporal representativeness error variance. Large values in θ^2 correspond to time periods with increased variability, as diagnosed by a wavelet analysis (d), particularly in the band between 2257 and 5298 year periods (grey lines). These periods correspond to $1/v_{\text{low}}^\dagger$ and $1/v_{\text{high}}^\dagger$, the reciprocals of the lower and upper cutoff frequencies for the power transfer function (dark blue curve, (c)). The light blue line in panel (c) indicates a power spectrum of the form $v^{-\beta}$ with $\beta = 1.53$ derived by a least-squares fit to the NGRIP spectrum.

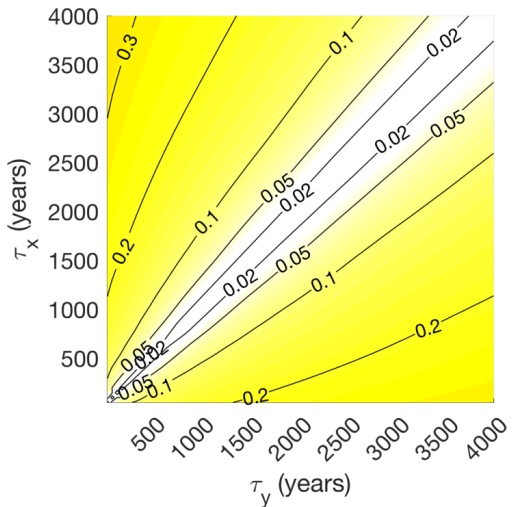


Figure 4: Error-to-signal variance fractions f (??) for estimates of time-mean values computed from the NGRIP record of Pleistocene oxygen isotopes contoured as a two-dimensional function of target averaging interval τ_x and observation averaging interval τ_y . A value of 0.1 means that TR error amplitudes are 10% of the “signal,” defined as the typical difference between two intervals separated by 21,000 years.

207 some time periods (including the LGM) are relatively small, whereas other times (e.g. 80-70 kya)
208 have larger errors and contribute more to $\langle \theta^2 \rangle$. This time-variability in errors arises from nonsta-
209 tionarities (changes in statistics) in the NGRIP oxygen isotope record, and points to a limitation in
210 our uncertainty quantification approach (which assumes stationarity). Information about nonsta-
211 tionarities, when available, should be used to inform error estimation, though we do not explore
212 that possibility here. Nevertheless, the estimate of $\langle \theta^2 \rangle$ is a reasonable characterization of typical
213 error variance.

Taking the square root of $\langle \theta^2 \rangle$ and normalizing by σ_{τ_0} , which is estimated by taking the square root of the lag τ_c autocovariance estimated over the NGRIP record, gives us the noise-to-signal ratio f for ranges of τ_x and τ_y between 10 and 4000 years (Figure ??). Errors are zero for $\tau_x = \tau_y$ and increase monotonically away from those values. Absolute errors $\langle \theta^2 \rangle$ are symmetric (i.e., equal if τ_x and τ_y are interchanged; not shown), but asymmetry in f arises because σ_{τ_0} depends on τ_x . TR errors can be up to 30% of signal amplitudes, with the largest errors occurring when a large τ_x is represented by a small τ_y .

3.2 Dependence on signal spectrum and archive smoothing

To investigate dependencies of TR error on signal spectra, we shift our focus from observations and assume power-law spectra for $r(t)$ having the form

$$|\hat{r}(v)|^2 \propto v^{-\beta}, \quad (22)$$

where $|\hat{r}(v)|^2$ is the power spectral density and β is the spectral slope (when plotted in log-log space, $v^{-\beta}$ is a straight line with slope $-\beta$). Spectra consistent with a power-law description are common in climate (?). Here we use as examples $\beta = 0.5$ and $\beta = 1.5$, motivated by ?, who fit paleoclimate records to spectral slopes between $\beta = 0.3$ and $\beta = 1.6$. Climatological spectral features that are not described by power laws, such as peaks due to the deterministic astronomical forcing from annual cycle or Milankovich variability, can also contribute to aliasing (??) but are not considered specifically here. All calculations are performed by numerical integration of Equation (??) by global adaptive quadrature.

Figure ?? shows the dependence of f on τ_x and τ_y varying τ_a to be 0 and 1000 years, and varying β to be 0.5 and 1.5. The close resemblance between Figure ??b (with $\beta = 1.5$) and the corresponding figure (??) computed in the time domain from NGRIP, which has spectral slope of 1.53, is partly coincidental; analysis of synthetic records with spectral slopes of 1.5 (not shown) reveals variability in f because of variations about the power law distribution in finite-length, stochastically generated time series. Nevertheless, a degree of agreement between the two cases is expected, and shows correspondence between time-domain and spectral approaches.

In the cases with no archive smoothing ($\tau_a = 0$, Figures ??a and ??b), errors are minimized for $\tau_x = \tau_y$ and increase monotonically away from those values. Errors are greatest for small values of τ_y and large values of τ_x , where TR error can dwarf relatively small signal amplitudes σ_{τ_c} typical of 21,000-year differences in long-term time averages. As spectra become more “red” (here, $\beta = 1.5$ rather than $\beta = 0.5$), σ_{τ_c} increases relative to $\langle \theta^2 \rangle$, and f decreases, as discussed also by ? and ?. Introducing archive smoothing (Figures ??a and ??c, shown for the case of $\tau_a=1000$), primarily

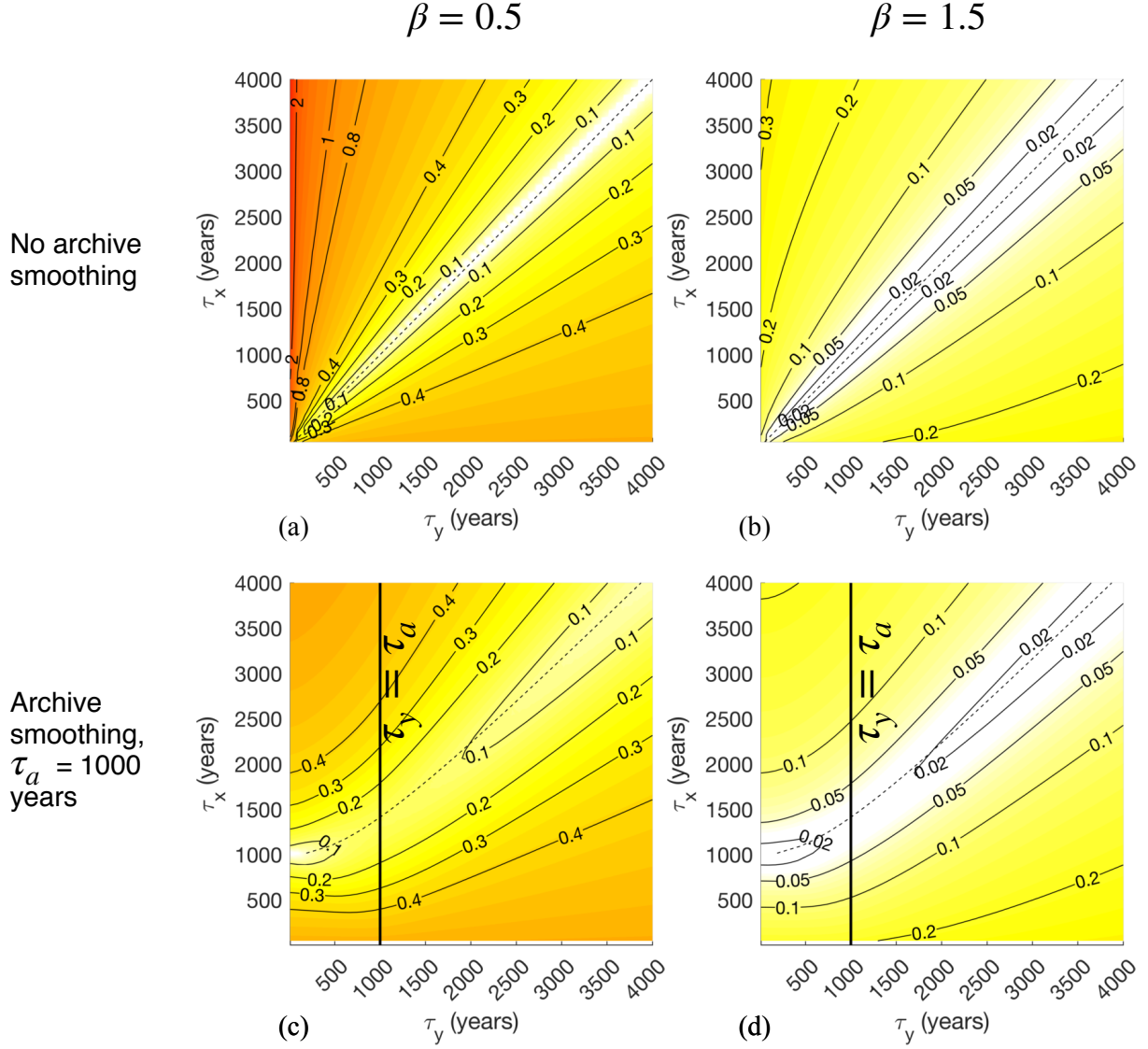


Figure 5: Error-to-signal fractions f for time-mean estimates plotted as a function of target averaging interval τ_x and observation averaging interval τ_y . Climate signal spectra are approximated as power law functions of frequency ($|\hat{r}(v)|^2 \propto v^{-\beta}$) with spectral slopes β equal to 0.5 (left column) and 1.5 (right column). The top row corresponds to a case with no archive smoothing ($\tau_a = 0$) while the bottom row corresponds to a case where the signal $r(t)$ is smoothed by a running mean over $\tau_a = 1000$ years. Time scales were chosen to be relevant to the problem of time-mean estimation at the Last Glacial Maximum, ca. 20 kya. Dotted lines show values of $\tilde{\tau}_y$ derived to minimize error estimated according to Equation (??).

245 affects f for $\tau_y < \tau_a$. In that regime, the largest values of f for small τ_y are reduced because
 246 archive smoothing serves as an anti-aliasing filter. Moreover, values of τ_y that minimize f change
 247 to reflect contributions from over-smoothing; for instance, when $\tau_x = 1000$, $\tilde{\tau}_y$ is close to zero.
 248 Observational averaging lengths τ_y that minimize f both with and without smoothing are well
 249 predicted by Equation (??) (dotted lines, Figure ??).

250 **3.3 Effects from known and unknown chronological offsets**

251 Offsets Δ between observed and target intervals aliases frequencies greater than $1/2\Delta$ onto the
 252 mean and modulates errors due to τ_x , τ_y , and τ_a (Section 2.2, Appendix A). Figure ?? illustrates
 253 these effects by computing f for $\tau_x = 4000$ years and varying Δ , τ_y , τ_a , and β . In all cases, errors
 254 grow monotonically away from $\Delta = 0$, $\tau_y = \tau_x$. For a given value of τ_y , the sensitivity of f to
 255 Δ (visible as a kink in contours, particularly in Figure ??a) increases for $\Delta > |\tau_x - \tau_y|/2$, when
 256 the observed time period begins to fall outside the target interval. As before, errors are more
 257 pronounced for $\beta = 0.5$ than for $\beta = 1.5$, with errors larger than the signal for small values of τ_y at
 258 all lags for $\beta = 0.5$, reflecting the smaller amplitude of aliased variability relative to σ_{τ_c} . Archive
 259 smoothing reduces f for $\tau_y < \tau_a$; for $\tau_y > \tau_a$, archive smoothing has no qualitative effect in the
 260 parameter range shown.

261 When the dating of a measurement is uncertain, a range of Δ values may be possible, as spec-
 262 ified by a probability distribution function $p(\Delta)$. To explore a scaling of the effects from chrono-
 263 logical uncertainty on representational error, we assume that $p(\Delta)$ is Gaussian about zero with
 264 standard deviation equal to the time scale σ_Δ . We then compute f as $\sqrt{\langle\langle\theta^2\rangle\rangle}/\sigma_{\tau_0}$, where $\langle\langle\theta^2\rangle\rangle$
 265 is given by numerical integration of Equation (??). In practice, $p(\Delta)$ can adopt a range of shapes,
 266 and in some cases (e.g., from radiocarbon ages; ?) can be non-Gaussian and / or bimodal, which
 267 would introduce additional time scales and could qualitatively change results. Such errors can be
 268 investigated by integrating Equation (??) with a non-Gaussian $p(\Delta)$.

269 Expected errors f as a function of σ_Δ and τ_y (Figure ??) are qualitatively similar to those for Δ

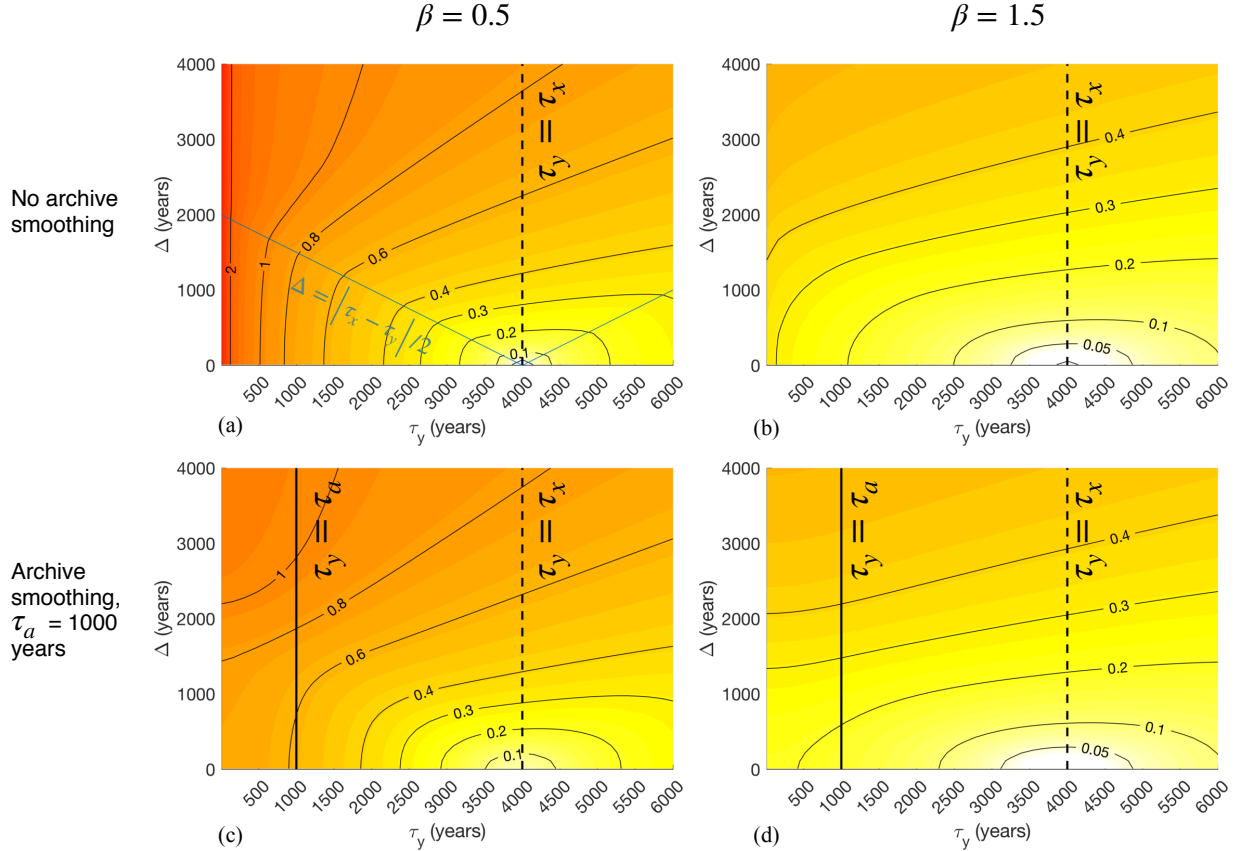


Figure 6: Same as Figure ??, but illustrating effects of offsets Δ between target and observational intervals on noise-to-signal ratios. Error fractions f are plotted as a function of the observational averaging interval τ_y and the standard deviation σ_Δ of a Gaussian distribution of observational offset centered on zero. In all cases, the target averaging interval is $\tau_x = 4000$, reflecting the nominal length of the Last Glacial Maximum. Values along the line $\tau_y = \tau_x$ strictly reflect the influence of chronological offsets. The blue line in panel (a) denotes values for which $\Delta = |\tau_x - \tau_y|/2$, indicating the maximum values of Δ for which τ_x and τ_y completely overlap.

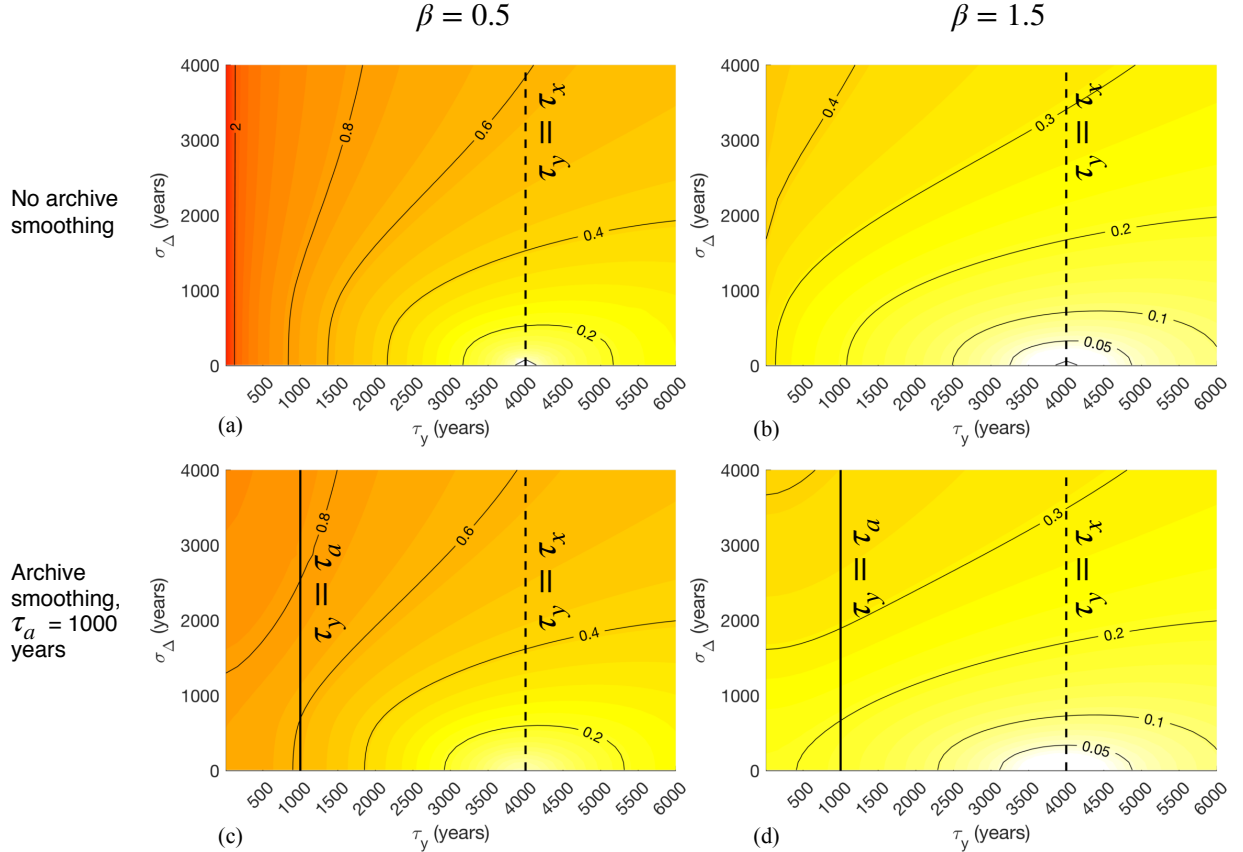


Figure 7: Same as Figure ??, but illustrating effects of chronological uncertainties in observations on noise-to-signal ratios. Error fractions f are plotted as a function of the observational averaging interval τ_y and the standard deviation σ_Δ of a Gaussian distribution of time offsets centered on zero. In all cases, the target averaging interval is $\tau_x = 4000$, reflecting the nominal length of the Last Glacial Maximum. Values along the line $\tau_y = \tau_x$ strictly reflect the influence of chronological uncertainty, which is zero when the observational offset is exactly known to be zero, (i.e., $\sigma_\Delta = 0$).

and τ_y (Figure ??), though values are everywhere slightly reduced, and the transition in sensitivity to σ_Δ across $\sigma_\Delta = |\tau_x - \tau_y|/2$ is less pronounced than for the equivalent in Figure ??, as might be expected given that a range of lags is possible for any nonzero σ_Δ . A consequence is that TR error arising from a chronological offset that is unknown, with standard deviation N years, is similar to the error arising from a known chronological offset of N years. This similarity holds in the presence of archive smoothing.

276 **4 Extension to time series analysis**

277 Paleoclimate time series are sequences of time-mean values. Just as sampling, archive smoothing,
278 and time offsets can introduce errors in estimates of time mean properties, so too do they introduce
279 errors in time series. However, these errors differ from the time mean case because, as discussed
280 below, uniform time mean measurements are not ideal for constructing time series. Here we adapt
281 the TR machinery to analyze individual measurements in paleoclimate time series. We show that
282 in the absence of archive smoothing, dense sampling (i.e., setting the averaging interval equal to
283 the spacing between measurements) is a nearly optimal approach to minimize TR errors.

284 The sampling theorem of ? states that sampling $r(t)$ instantaneously (that is, with a very short
285 averaging interval) at times separated by a fixed time interval τ_s unambiguously preserves signal
286 information only when $r(t)$ does not contain any spectral power at frequencies greater than $1/2\tau_s$
287 (called the Nyquist frequency, v_{Nyq}). When this criterion is not met, the discrete signal is corrupted
288 by aliasing, whereby variability in $r(t)$ at frequencies greater than v_{Nyq} appears artificially at lower
289 frequencies in the discrete signal. To mitigate aliasing, one can either increase the sampling rate or
290 apply a low-pass “anti-aliasing” filter to $r(t)$ to attenuate power at frequencies higher than v_{Nyq} . In
291 the process of constructing a paleoclimate time series, sampling time-mean values yields a moving
292 average that serves as an anti-aliasing filter. Thus we expect sample averaging procedures to affect
293 aliasing errors in time series, as also discussed by ?.

294 We will use Shannon’s theorem to obtain an expression for TR errors for individual time series
295 measurements. Our procedure is to define local values of τ_s^i and v_{Nyq}^i for the i^{th} observation and
296 compute the expected errors if an entire time series were sampled using those local properties. We
297 make the assumption that the sampling interval τ_s^i is locally constant: that is, for the i^{th} measure-
298 ment y^i taken at time t^i , y^{i-1} was taken at time $t^i - \tau_s^i$, and y^{i+1} was taken at time $t^i + \tau_s^i$. If the
299 sampling interval changes rapidly, conclusions from this approach might not apply.

300 Define the moving average time series associated with y^i to be

$$y^i(t) = \Pi(t, \tau_y^i) \star \Pi(t, \tau_a^i) \star r(t) \quad (23)$$

301 where we have included a contribution from archive smoothing, so that its Fourier transform is

$$\hat{y}^i(\nu) = \hat{\Pi}(\nu, \tau_y^i) \cdot \hat{\Pi}(\nu, \tau_a^i) \cdot \hat{r}(\nu). \quad (24)$$

302 By Shannon's theorem, an accurate discrete representation of $r(t)$ results from sampling all fre-
 303 quencies in $r(t)$ less than or equal to the local Nyquist frequency $\nu_{Nyq}^i = 1/(2\tau_s^i)$. As such, the
 304 target value x^i for the i^{th} measurement y^i is the value of $r(t)$ sampled at t^i after filtering $r(t)$ to
 305 remove high-frequency variability. The Fourier transform of a time series of values of x^i is

$$\hat{x}^i(\nu) = G(\nu, \tau_s^i) \hat{r}(\nu) \quad (25)$$

306 where the “ideal” transfer function $G(\nu, \tau_s)$ is the piecewise constant Heaviside function

$$G(\nu, \tau_s) = \begin{cases} 1 & \nu < 1/(2\tau_s^i) \\ 0 & \nu \geq 1/(2\tau_s^i) \end{cases} \quad (26)$$

307 that is ideal in the sense that it eliminates variability at frequencies greater than $\nu_{Nyq}^i = 1/(2\tau_s^i)$.
 308 Then we define TR error at the i^{th} measurement to be

$$\theta^i = x^i - y^i. \quad (27)$$

309 As in the previous section, we estimate the variance of θ^i by taking the expected value as if the
 310 entire record had been sampled using the local values τ_s^i and τ_y^i . Then, equivalent to (??),

$$\langle \theta^{i2} \rangle = \frac{1}{\tau_0} \int_0^\infty |G(\nu, \tau_s^i) - \hat{\Pi}(\nu, \tau_a^i) \cdot \hat{\Pi}(\nu, \tau_y^i)|^2 |\hat{r}(\nu)|^2 d\nu. \quad (28)$$

311 Similar to the time-mean case, $\langle \theta^{i2} \rangle$ is a weighted integral over the power density spectrum of
 312 $r(t)$. Weights are largest at frequencies between ν_{Nyq} and either ν_{low}^\dagger (if $\tau_y > \tau_s$) or ν_{high}^\dagger (if $\tau_y < \tau_s$).
 313 Unlike in the mean estimation case, where TR errors can be zero, nonzero error is unavoidable with

314 uniform sampling because of differences between the shape of the sinc function and the abrupt
315 frequency cutoff specified by $G(v, \tau_s^i)$. Sampling a paleoclimate archive nonuniformly in time
316 could better approximate the ideal filter and reduce errors, but this may not be practical given the
317 many other sources of error in paleoclimate records.

318 To demonstrate sensitivities to parameters we again compute noise-to-signal ratios. We take
319 signal strength to be the estimated standard deviation $\tilde{\sigma}_{x^i}$ of the time series of x^i , so that the noise-
320 to-signal ratio at the i^{th} measurement is

$$f^i = \frac{\sqrt{\langle \theta^{i2} \rangle}}{\tilde{\sigma}_{x^i}}.$$

321 Because $\tilde{\sigma}_{x^i}$ can grow as a function of time series length for power-law spectra, we choose 21,000
322 years as the period over which to integrate signal variance, the approximate duration of the last
323 deglaciation.

324 While the dependence of f^i on τ_s^i and τ_y^i (Figure ??) is qualitatively similar to the dependence
325 on τ_x and τ_y in the time mean estimation case (Figure ??), there are some differences. First, as
326 discussed above, errors are always 10% or more of signal amplitudes. Second, values of τ_y that
327 minimize errors do not obey $\tau_y = \tau_s$, but are larger by a factor of roughly 1.2, suggesting that
328 samples should ideally span an interval slightly longer than the sampling interval. In practice,
329 sampling densely (without space between observations) would seem to be a good approximation
330 of this error minimizing strategy. For time series constructed from short time averages spaced out
331 by larger intervals in time, errors can be large relative to climate signals.

332 As stated above, these results hold for time series whose spacing and chronologies are not
333 changing too rapidly and where the goal is to obtain a discrete representation of a continuous
334 process. For other objectives, other sampling procedures may be preferred. For instance, “burst
335 sampling,” whereby rapid sequences of observations are taken at relatively long intervals, is used in
336 modern oceanographic procedures to estimate spectral nonstationarities in time (?), and unevenly
337 spaced paleoclimate observations can be leveraged to give a range of frequency information using

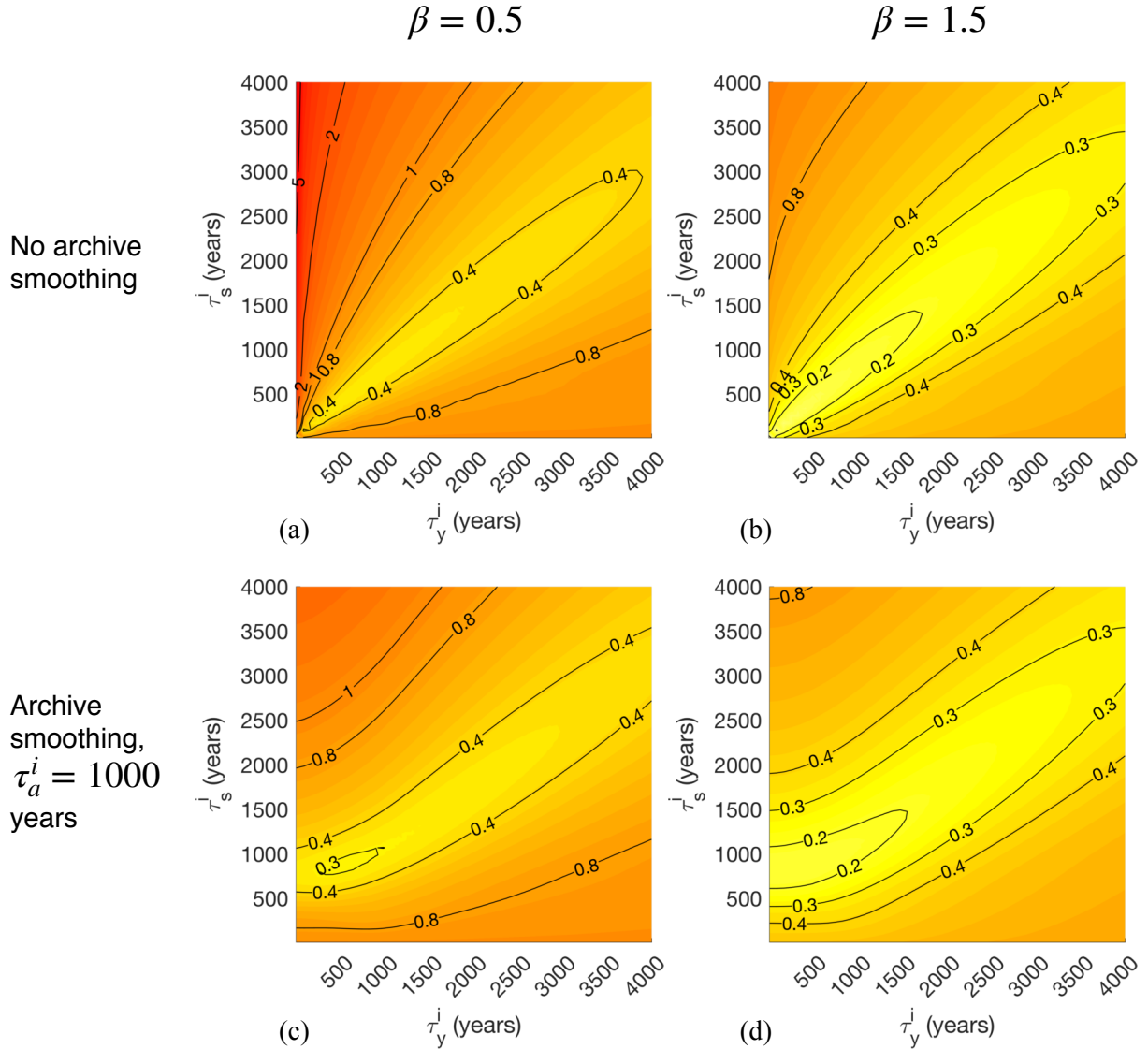


Figure 8: Same as Figure ??, but illustrating the dependence of the error-to-signal standard deviation ratio for individual measurements in a time series as a function of local time series spacing (τ_s^i) and the observational averaging time interval τ_y^i .

338 variogram approaches (?) or the Lomb-Scargle periodogram (e.g., ?). The danger of aliasing is
339 omnipresent, and necessitates careful consideration of the frequencies sampled by an observation
340 and the frequencies the observation is being used to constrain.

341 5 Discussion

342 This paper presents a framework for quantifying temporal representativeness (TR) errors in paleo-
343 climate, broadly defined as resulting when one time average is represented by another. A simple
344 model illustrates interacting effects from record sampling procedures, chronological errors, and
345 the spectral properties of the climate process being sampled.

346 Uncertainty quantification is important for interpreting records, comparing them to other data,
347 and incorporating them into reconstructions using inverse modeling or data assimilation approaches.
348 For instance, uncertainties play a crucial role in determining how observations influence least-
349 squares reconstructions of past climate: highly uncertain observations carry little weight, while
350 those with low uncertainty have more power in dictating reconstruction features (e.g., discussions
351 in ??). In data intercomparisons, differing sampling strategies could contribute to disagreement
352 among paleoclimate records obtained from different archives, while sampling errors could be cor-
353 related measurements obtained from a single set of samples, possibly leading to apparently better
354 agreement of properties within than between archives.

355 We find that for some cases of sampling time scales, archive smoothing, and climate spec-
356 tra, TR errors are non-negligible, with noise-to-signal ratios greater than 1 in some cases where
357 the observational interval τ_y is smaller than the target interval τ_x . TR errors result from aliasing
358 climate variability onto time mean observations and can be mitigated to some degree by sam-
359 pling procedures and by archive smoothing, both of which act as anti-aliasing filters. However,
360 archive smoothing can also destroy information about climate variability, and the combined effects
361 of sampling and smoothing can over-smooth a record and lead to increased errors. The effects
362 from mismatches between τ_x and τ_y have similar amplitudes to uncertainties from chronological

363 errors in the parameter space considered. Moreover, chronological and sampling errors interact, for
364 instance in the way that errors grow more quickly as a function of chronological uncertainty ampli-
365 tude when that uncertainty is likely to place a measurement outside of a target interval (Figure ??).
366 Given that these error variances were estimated using parameters representative of the LGM, it
367 seems possible that TR errors may explain some of the disagreement among proxy measurements
368 within that time period (e.g., ??). Importantly, we do not claim that TR errors are the largest
369 source of error for any particular proxy type or reconstruction problem, though they may well be.
370 The tools presented can be used to assess how large errors are likely to be.

371 Though not the principal goal, these analyses provide a basis for sampling practices that min-
372 imize errors, notably for avoiding oversmoothing through the combined effects of sampling and
373 archive smoothing (Section ??). When constructing paleoclimate time series, it is important to
374 bear in mind not just the Nyquist frequency but its interaction with sample lengths in time; these
375 considerations point to dense sampling (i.e., without space between contiguous samples) in order
376 to minimize error (Section ??). However, many practical considerations motivate paleoclimate
377 sampling strategies, and may outweigh the concerns described here. For instance, records sampled
378 densely cannot be used as a starting point for subsequently constructing higher-resolution records.
379 Moreover, preservation of natural archives for subsequent analyses is important for reproducibility
380 and for sharing resources between laboratories, and may be complicated by continuous sampling.

381 To some extent, the simple model for TR error can be generalized to more complex scenarios.
382 If samples are nonuniform in time – for instance, due to large changes in chronology, or because
383 material was sampled using a syringe or drill bit with a circular projection onto the archive – then
384 the sinc function in (??) can be replaced by Fourier transforms of the relevant functions. Similarly,
385 a more complex pattern of archive smoothing can be accommodated by substituting a different
386 smoothing kernel. Non-Gaussian age uncertainties can be incorporated by substituting a different
387 distribution in (??). Changes in sampling properties through time (as might arise from non-constant
388 chronologies or sampling procedures) can readily be accommodated because all computations are
389 performed on a point-by-point basis. If time scales (e.g., τ_a) are unknown, a similar procedure can

390 be adopted as was used for Δ in (??), whereby a second integration is performed to compute the
391 expectation over an estimated probability distribution.

392 Several caveats apply to the uncertainty estimates. First, we assume that proxy archives store
393 information continuously, thereby neglecting errors due to small numbers of foraminifera in sedi-
394 ment cores or particle size sorting in diagenesis. Second, nonstationarity in record spectra leads to
395 time variations in errors, as illustrated in Figure ???. Third, by estimating errors for individual mea-
396 surements, we ignore error covariances in time, which can result from chronologies constructed
397 by interpolating ages between tie points; more complete characterizations could be achieved by
398 Monte Carlo sampling of age model uncertainty (e.g., ?). More broadly, there is clear need for
399 comprehensive approaches in uncertainty quantification that can reveal interactions among the
400 various sources of uncertainty in paleoclimate records. Forward proxy system models (???) are a
401 promising way forward to assess uncertainties holistically.

402 Aliasing is not limited to the time domain, and similar procedures may be useful for quantifying
403 errors due to spatial representativeness by considering how well proxy records can constrain the
404 regional and larger scales typically of interest in paleoclimatology. An analogous problem is ad-
405 dressed in the modern ocean by ?, and ? considered spatial representativeness in choosing how to
406 weight deglacial radiocarbon time series in spatial bin averages. A challenge of any such approach
407 is that the spatial averaging functions (analogous to our τ_y , but occupying three spatial dimensions)
408 represented by proxy records are often not well known; ?, for instance, explores how ocean advec-
409 tion determines three-dimensional patterns represented by sediment core observations. Because
410 spatial patterns and time scales of ocean and climate variability are linked, it may ultimately be
411 necessary to consider the full, four-dimensional spatiotemporal aliasing problem.

412 The hope is that these procedures may prove useful for first-order practical uncertainty quantifi-
413 cation, and scripts and functions used in making figures are provided (see link in the Acknowledge-
414 ments). A challenge is estimating the signal spectrum $|\hat{r}|^2$, which itself can be affected by aliasing
415 (?). One approach is to use spectra from other records that are more highly-resolved or were sam-
416 pled densely, e.g. from a sediment core at an adjacent site, or a record believed to record similar

417 climate variability. Alternately, measurements of archive properties that can be made cheaply and
 418 at high resolution – such as magnetic susceptibility, wet bulk density, and other proxy properties
 419 that are routinely made on sediment cores – could prove useful for estimating $|\hat{r}|^2$ if those prop-
 420 erties are related linearly to $r(t)$ (??). Another challenge is that time scales that we have shown
 421 affect errors are often not published alongside paleoclimate datasets, thus turning systematic errors
 422 (where parameters like τ_y are known) into stochastic errors because a range of possible values must
 423 be explored. Publishing all available information about sampling practices, age model construc-
 424 tion, and assessments of archive smoothing will greatly aid uncertainty quantification efforts.

425 **6 Appendix 1: Expressing temporal representativeness errors 426 in the frequency domain**

427 The Fourier transform will be written using the operator \mathcal{F} and by a hat, and denoting frequency
 428 by v ,

$$\mathcal{F}(x(t)) \equiv \hat{x}(v) = \int_{-\infty}^{\infty} x(t) e^{-2\pi i v t} dt.$$

Parseval's theorem states that the integral of a squared quantity in the time domain is equal to the
 integral of the squared amplitude of the Fourier transform of that quantity, so that we can write
 (??) as

$$\langle \theta^2 \rangle = \frac{1}{\tau_0} \int_{-\infty}^{\infty} (m(t, \tau_x) - m(t + \Delta t, \tau_y))^2 dt \quad (29)$$

$$= \frac{1}{\tau_0} \int_0^{\infty} |\mathcal{F}[m(t, \tau_x) - m(t + \Delta t, \tau_y)]|^2 dv. \quad (30)$$

429 By the Fourier shift theorem,

$$\mathcal{F}[m(t + \Delta, \tau_y)] = e^{-2\pi i v \Delta} \mathcal{F}[m(t, \tau_y)]. \quad (31)$$

⁴³⁰ Then, by the linearity of the Fourier transform,

$$\langle \theta^2 \rangle = \frac{1}{\tau_0} \int_0^\infty \left| \hat{m}(v, \tau_y) - e^{-2\pi i v \Delta} \hat{m}(v, \tau_x) \right|^2 dv. \quad (32)$$

By the convolution theorem, convolution in the time domain is equivalent to multiplication in the frequency domain, and vice versa. Thus, the Fourier transform of a time mean as defined in (??) is

$$\hat{m}(v, \tau) = \mathcal{F}[\Pi(t, \tau) \star r(t)] \quad (33)$$

$$= \hat{\Pi}(v, \tau) \cdot \hat{r}(v). \quad (34)$$

Substituting into (??) yields

$$\langle \theta^2 \rangle = \frac{1}{\tau_0} \int_0^\infty \left| \hat{\Pi}(v, \tau_x) - e^{-2\pi i v \Delta} \cdot \hat{\Pi}(v, \tau_y) \right|^2 |\hat{r}(v)|^2 dv. \quad (35)$$

⁴³¹ We can represent smoothing prior to sampling by substituting a new climate signal, $r(t)$, with a
⁴³² running mean applied,

$$r'(t) = \Pi(t, \tau_a) \star r(t).$$

⁴³³ Substituting $\hat{r}'(v)$ into (??) and applying the convolution theorem gives

$$\langle \theta^2 \rangle = \frac{1}{\tau_0} \int_0^\infty \left| \hat{\Pi}(v, \tau_x) - \hat{\Pi}(v, \tau_a) \cdot \hat{\Pi}(v, \tau_y) \right|^2 |\hat{r}(v)|^2 dv. \quad (36)$$

To isolate the effect of a time offset Δ , consider the limit where τ_x , τ_y , and τ_a approach zero, corresponding to instantaneous observations in time, so that $\langle \theta^2 \rangle$ approaches

$$\langle \theta^2 \rangle = \frac{1}{\tau_0} \int_0^\infty \left| 1 - e^{-2\pi i v \Delta} \right|^2 |\hat{r}(v)|^2 dv. \quad (37)$$

Expanding $|1 - e^{-2\pi i v \Delta}|^2$ and simplifying gives

$$\langle \theta^2 \rangle = \frac{1}{\tau_0} \int_0^\infty (2 - 2 \cos(2\pi v \Delta)) |\hat{r}(v)|^2 dv \quad (38)$$

so that the power transfer function is $H = 2 - 2 \cos(2\pi v \Delta)$ and the expected error due to Δ is a cosinusoidally-weighted function of the signal power spectrum. H takes a minimum value of 0 at frequencies

$$v_{min} = 0, \frac{1}{\Delta}, \frac{2}{\Delta}, \dots, \frac{n}{\Delta}$$

for integer values of n ; at these frequencies, measurements spaced by Δ in time are in phase and are therefore exactly correlated (Figure ??a). The weights take a maximum value of 4 at frequencies

$$v_{max} = \frac{1}{2\Delta}, \frac{3}{2\Delta}, \frac{5}{2\Delta}, \dots, \frac{n}{\Delta} + \frac{1}{2\Delta}$$

where measurements separated by Δ are always exactly out of phase (Figure ??b). At those frequencies, the underlying signal $r(t)$ is projected twofold onto the error, so that its variance contribution is multiplied fourfold. These variations in frequency contributions to error modulate effects from smoothing and sampling timescales, as illustrated in Figure ??.

443 Acknowledgements

Thanks to LuAnne Thompson, Greg Hakim, Lloyd Keigwin, Cristi Proistescu, Carl Wunsch, and Thomas Laepple for useful conversations and comments. Support came from NOAA grant XXXX and an NSF postdoctoral fellowship. Wavelet software was provided by C. Torrence and G. Compo, and is available at URL: <http://paos.colorado.edu/research/wavelets/>. MATLAB code to integrate these equations and reproduce Figure ?? is available at https://github.com/amrhein/Temporal_representation

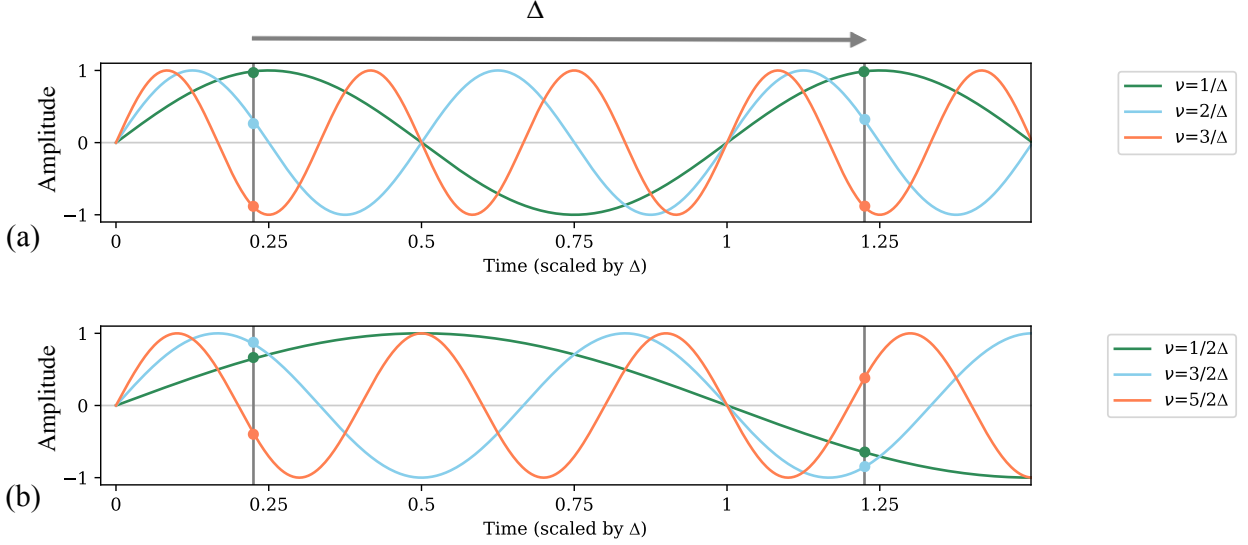


Figure 9: Illustration of the frequency dependence of errors in representing an instantaneous measurement of a process $r(t)$ at a time t by another measurement $r(t + \Delta)$. Each line represents a different frequency component of $r(t)$, grey vertical lines represent sampling times, and colored circles represent values of components at those times. At frequencies $v = \frac{n}{\Delta}$ for $n = 0, 1, 2, \dots$, (a), the Fourier components of $x(t)$ will be exactly in phase when sampled at a time lag Δ , so these components do not contribute to the error variance $\langle (r(t) - r(t + \Delta))^2 \rangle$. By contrast, at frequencies $v = \frac{n}{\Delta} + \frac{1}{2\Delta}$ (b), the Fourier components are exactly out of phase, so these components tend to contribute most to the error variance. At intermediate frequencies, contributions lie between the two extremes, leading to a cosine function of error contribution as a function of frequency (Equation ??).